Discover Oncology

Research

The interplay between angiogenesis-associated genes and molecular, clinical, and immune features in bladder cancer

Xiaoxiao Guo[1,2] · Jingxin Yang[3,4] · Rui Cao[1] · Gangyue Hao[1,2]

Received: 17 July 2024 / Accepted: 11 February 2025
Published online: 05 March 2025

Abstract

Background Immunotherapy plays an important role in the treatment of bladder cancer (BLCA), with outcomes influenced by the tumor microenvironment (TME). Angiogenesis, a hallmark of cancer progression, shapes the TME and impacts immunotherapy efficacy. However, its specific role in BLCA remains underexplored.

Methods We analyzed 268 angiogenesis-related genes (ARGs) across ten gene sets using data from The Cancer Genome Atlas (TCGA) and Gene Expression Omnibus (GEO) cohorts. Through unsupervised clustering, we identified ARG-based subtypes and developed an ARG scoring system to quantify angiogenesis activity. The ARG score was correlated with clinical outcomes, immune cell infiltration, and immunotherapy response. Functional validation was performed using in vitro assays.

Results Two distinct ARG clusters exhibited significant differences in immune profiles, clinical outcomes, and functional characteristics. Patients in the high ARG cluster had poorer survival but showed enhanced responsiveness to immune checkpoint inhibitors (ICIs). The novel ARG score demonstrated strong predictive power for immunotherapy efficacy and survival outcomes.

Conclusion ARG expression patterns profoundly impact the TME, clinical outcomes, and immunotherapy response in BLCA. The ARG score is a novel biomarker for stratifying patients and optimizing treatment strategies. These findings may contribute to clarifying the characteristics of TME and enable the exploration of more potent immunotherapy strategies.

Keywords Bladder cancer · Angiogenesis-associated genes · Angiogenesis score · Tumor microenvironment · Tumor prognosis

Xiaoxiao Guo, Jingxin Yang are contributed equally as first authors.

Supplementary Information The online version contains supplementary material available at https://doi.org/10.1007/s12672-025-01966-w.

✉ Xiaoxiao Guo, ensitern@163.com; ✉ Gangyue Hao, haogangyue@126.com | [1]Department of Urology, Beijing Friendship Hospital, Capital Medical University, Beijing 100050, China. [2]Institute of Urology, Beijing Municipal Health Commission, Beijing, China. [3]Department of Urology, National Center of Gerontology, Beijing Hospital, Beijing, China. [4]Medical School, University of Chinese Academy of Sciences, Beijing, China.

1 Background

Bladder cancer (BLCA) is one of the most prevalent malignancies within the urological system [1]. Over the past two decades, platinum-based chemotherapy has remained a cornerstone in the pharmacological treatment of BLCA. The emergence of immune checkpoint inhibitors (ICI) has paved a new way for therapeutic of BLCA, and recent research indicates promising outcomes with ICI in the treatment of muscle-invasive BLCA patients [2, 3]. However, owing to the unique clinical and molecular characteristics of individuals, the effectiveness of immunotherapy is varies [4, 5]. The tumor immune microenvironment (TME) plays a crucial role in influencing the outcomes of immunotherapy. Therefore, investigating the factors affecting TME characteristics in BLCA is of paramount importance in enhancing the efficacy of immunotherapy.

Angiogenesis plays a pivotal role in promoting tumor initiation and progression, as evidenced by the upregulation of angiogenic factors in various malignancies [6]. For certain tumors with limited therapeutic options, inhibiting angiogenesis has proven to be an effective treatment strategy [6, 7]. Recent studies underscore the regulatory role of angiogenesis within the tumor immune microenvironment, encompassing antigen presentation, activation of cytotoxic CD8 + T cells, as well as lymphocyte infiltration and migration [8, 9]. These findings suggest the impact of angiogenesis-related genes (ARGs) on TME. However, existing research predominantly focuses on describing the individual effects of single angiogenesis genes on BLCA progression and prognosis. In this study, we leveraged data from The Cancer Genome Atlas (TCGA) and Gene Expression Omnibus (GEO) datasets to analyze a panel of ARGs in BLCA and explored the implications of this gene set's expression on TME, drug treatment responses, and tumor prognosis. Furthermore, we devised an ARG scoring system to assess its relationship with the effectiveness of immunotherapy and predictive capabilities for patient's survival. This research endeavor to elucidate the intricate interplay between ARGs and TME, aiding in the formulation of more personalized and efficacious treatment strategies for BLCA patients.

2 Materials and methods

2.1 Data collection

Our study incorporated three GEO cohorts (GSE31684, GSE48276, and GSE13507) that were merged with the TCGA-BLCA cohort to create a meta-BLCA cohort. Samples lacking complete prognosis information were excluded from further evaluation. The raw data from the GEO database were processed using the robust multi-chip averaging algorithm for background correction, log2 transformation, and subsequent quantile normalization. The level 3 RNA-sequencing data for fragments per kilobase of transcript per million (FPKM) mapped reads for gene expression in the TCGA-BLCA dataset were downloaded from the TCGA Genomic Data Commons data portal (https://portal.gdc.cancer.gov/). Then, FPKM values were transformed into transcripts per kilobase million, which are more similar to gene expression from microarrays and more comparable between samples. Gene expression was annotated with the highest expression value when multiple probes or Ensemble IDs were mapped to a single gene symbol in the RNA-sequencing data. The ComBat algorithm of package "sva" in R was utilized to reduce the likelihood of batch effects of non-biological technical biases from each dataset [10]. A total of 268 genes were obtained from ten independent angiogenesis gene sets, and we identified differentially expressed genes and prognostically relevant genes from these sets (Supplement Table 1). The TCGA cohort was used to identify the different expression genes (DEGs) between normal and tumor tissues, with the "limma" package utilized to identify DEGs having a P-value <0.01. To assess the prognostic value of the angiogenesis-related genes, we further employed Cox regression analysis to examine the correlations between each gene and overall survival (OS) in the TCGA cohort, using a cut-off P-value of 0.05.

2.2 Unsupervised consensus clustering analysis of ARGs

Consensus clustering based on k-means algorithms was employed to define distinct angiogenesis-related patterns [11]. The quantity, as well as the consistency of clusters, was built by the consensus clustering algorithm, which is available in the 'Consensus Cluster Plus' package [12]. 1000 iterations were performed to ensure the stability of these

categories. To identify the biological functional differences in ARGs, gene set variation analysis (GSVA) was conducted with the Kyoto Encyclopedia of Genes and Genomes (KEGG) gene set [13].

2.3 Association between ARG clusters with the clinical characteristics and prognosis of BLCA

To ascertain the clinical significance of ARG clusters, we investigated the relationship between ARG clusters and clinical characteristics (age, gender, tumor grade, T stage, N stage, and M stage), as well as survival outcomes. Moreover, differences in OS between different clusters were evaluated with Kaplan–Meier analysis.

2.4 Relationship of ARG clusters with TME in BLCA

The infiltrating fractions of immune cells were identified with a single-sample gene set enrichment analysis (ssGSEA) algorithm. Subsequently, we assessed the correlation between ARG clusters and the expression of PD-1, PD-L1, and CTLA-4. The ESTIMATE algorithm was employed to evaluate the immune and stromal scores for patients with bladder cancer (BLCA), providing an estimation of the relative proportions of immune and non-immune components within the tumor microenvironment [14]. Subsequently, the CIBERSORT algorithm was utilized to calculate the levels of 22 distinct immune cell subtypes for each patient. This allowed for a detailed characterization of the composition of immune cells present in the TME [15].

2.5 Identification of DEGs in ARG clusters and functional enrichment analysis

To identify DEGs in the distinct ARG Clusters, we used the "limma" package with criteria of |log2-fold change (FC)| ≥ 1 and p-value < 0.05. Based on these DEGs, GO and KEGG analysis was carried out with the "clusterProfiler" package. Next, we conducted univariate Cox regression (uniCox) analysis for DEGs. Survival-related genes were retained for further analysis.

2.6 Development of the angiogenesis related gene prognostic score

Then, LASSO Cox regression analysis based on the package "glmnet" in R was applied to build an optimal survival prognostic signature for BLCA by using the DEGs mentioned above. The Cox regression model with LASSO was used for dimension reduction to reduce noise or redundant genes. The optimal values of the penalty parameter λ were determined through 10 cross-validations. The ARG score for each sample in our model was defined by the expression of each ARG and its associated Cox coefficient. The ARG score = $\Sigma_{i=1}^{n}$ (coefi × Expri), where Expri is the expression of the gene in the signature for patient i and coefi is the LASSO Cox coefficient of gene i. According to the ARG score, we grouped all patients into low or high score groups at the median cut-off in each cohort. To reflect the prediction accuracy and ability of the builded model, the area under the curve (AUC) for 3-year, 5-year and 10-year OS was measured through time-dependent receiver operating characteristic (ROC) curve analysis using the package "survivalROC" in R. K–M survival analysis was employed to compare between the high-score group and the low-score group. The relevance of the ARG score to immune cells was investigated. Furthermore, the infiltrating levels of immune cells and immune checkpoint (ICP) were compared in the different ARG score groups.

2.7 Mutation and drug sensitivity analysis

To identify the mutational profiles of BLCA patients between different ARG score groups, the TCGA-BLCA somatic mutation data, which were identified using MuTect2, were obtained from UCSC Xena (https ://tcga.xenah ubs.net). The called somatic variants determined by TCGA were utilized as the raw mutation count. Mutation status was analyzed and visualized by the packages "maftools" in R [16]. Then, the tumor mutational burden (TMB) per megabase of each sample was calculated as the total number of mutations counted in the exome territory. An estimate of the exome size was 38 Mb according to a previous study [17]. The immunophenotype score (IPS) for BLCA patients in the two ARG clusters were also assessed. To investigate the clinic performance of chemotherapy agents in patients, the semi-inhibitory concentration (IC50) values of common chemotherapy drugs for BLCA were calculated with the "pRRophetic" package [18].

2.8 Establishment of a predictive nomogram

A nomogram and calibration curves based on their ARG scores and other clinicopathological characteristics were generated with the packages 'rms', 'nomogramEx', and 'regplot' in R, aiming to provide valuable clinical predictions for BLCA patients, particularly for 3-, 5-, and 10-year OS. Decision curve analysis (DCA) was performed to determine whether our established nomogram was suitable for clinical use according to the suggestion of Iasonos et al. [19]. Supplement Figure 1 shows the complete analysis process for this study.

2.9 Cell culture and transfection

We obtained the human bladder cancer cell line 5637 from the Cell Bank of the Typical Culture Collection of the Chinese Academy of Sciences. These cell lines were cultured in DMEM supplemented with 10% FBS and 1% penicillin-streptomycin, and maintained at a temperature of 37 °C in a 5% CO_2 atmosphere. Ribobio (Guangzhou, China) was commissioned to synthesize small interfering RNA (si-RNA) and its negative control (si-NC). The target sequences of siRNA for CD109 were 5′–CGCTTATCA TTTGAGACCAAGAGAA (si-CD109), and for TM4SF1, 5′–CGCTTATCATTTGAGACCAAGAGAA. The cells were treated with si-RNA or si-NC using Lipofectamine 3000 following the protocol provided by the manufacturer (Invitrogen; Carlsbad, CA, USA).

2.10 RNA extraction and quantitative teal-time PCR (qRT-PCR)

The total RNA was isolated from cells or tissues using TRIzol (15,596,018, Thermo, Waltham, MA, USA). The quantity and quality of RNA were determined spectrophotometry, followed by reverse transcription into cDNA using the PrimeScript™ RT reagent kit (R232-01, Vazyme, Nanjing, China). qRT-PCR was then conducted on the LightCycler 480 Real-Time PCR System (Roche Diagnostics, Basel, Switzerland), with GAPDH serving as the internal control for selected genes. To calculate the level of genes, the $2^{-\Delta\Delta CT}$ method was used. All primers used for qRT-PCR were produced by Tsingke Biotech (Tsingke, Beijing, China), and the following is a list of primer sequences: CD109 forward: CCTCCTAATACAGTGACTGGCAG; reverse: CTGTTCACCACAGCC ATAAGGC; TM4SF1 forward: GGCTACTGTGTCATTGTGGCAG, reverse: ACTCGGACCATGTGGAGGTATC; GAPDH Forward: GGC CTCCAAGGAGTAAGACC; Reverse: AGGGGAGATTCAGTGTGGTG.

2.11 Cell proliferation and invasion assay

We utilized the Cell Counting Kit-8 (CCK-8) assay to explore cell proliferation. The transfected cells were planted at a density of 2000 cells/well in a 96-well plate overnight (at 37 °C with 5% CO2). The cells were incubated with 10 µL of CCK-8 labelling reagent (A311- 01, vazyme, Nanjing, China) and 90 µL of serum-free medium per well in darkness at 37 °C for 2 h. Absorbance was determined at a wavelength of 450 nm using an enzyme-labelled meter (A33978, Thermo, Waltham, MA, USA). Concerning the colony formation experiment, about 500 transfected cells were seeded into each well of the 6-well plate and given time to form into colonies. Next, cells were washed with PBS and fixed with 4% paraformaldehyde for 15 min. Staining crystalline violet for 20 min, allowing it to dry at room temperature, and then counting the number of cells under an inverted microscope yielded the desired results. Transwell migration and wound healing assays are used to explore cell proliferation. In a 24-well transwell plate, 5637 cells were resuspended in 200 µL medium without FBS and inserted into the upper chamber, while 600 µL of medium containing 10% FBS was placed in the lower chamber. Invasion and migration assays were conducted with or without Matrigel coating on the transwell chamber (2 mg/ml, BD Biosciences, Franklin Lakes, NJ, USA). Non-invasive cells were eliminated from the top of the membrane after 48 h, whereas invasive cells were fixed with 4% paraformaldehyde and stained with 0.1% crystal violet (Solarbio, Beijing, China). Three different fields of cells were photographed and counted at 200x magnification using a light microscope. Transfected 5637 cells were cultured in 6-well plates containing DMEM-free of FBS, and linear wounds were scratched with a 200 µL pipette tip for the wound healing assay. After scratching, cell migration was assessed and photographed at fixed positions at 0 and 48 h under an inverted microscope.

2.12 Statistical analysis

The statistical significance of variables between two groups was estimated by Student's t tests or Wilcoxon tests. In addition, for variables in more than two groups, one-way ANOVA or Kruskal–Wallis tests were used. The $\chi 2$ test was applied to analyze correlations between the gene clusters and clinicopathological parameters. Correlation coefficients between

TME-infiltrating immune cells, distinct gene sets, and the ARG score were computed by Pearson and distance correlation analyses. A two-sided Fisher's exact test was used to analyze contingency tables. Univariate and multivariate Cox proportional hazard models were used to estimate the hazard ratios (HRs) of variables and determine independent prognostic factors and were visualized with the package "forestplot" in R. A waterfall plot was used to present the mutation landscape in patients with distinct hypoxia response phenotypes in TCGA-BLCA cohort via packages "maftools" [16] in R. The area under the curve and confidence intervals were utilized to evaluate the diagnostic accuracy of clinicopathological parameters and clinicopathological parameters combined with ARG score. For RNA differential expression analysis, p-values were adjusted using the false discovery rate (FDR) method, with an FDR threshold set at 0.05. All statistical analyses were performed with R software 4.1.2. Statistical significance was set at $p < 0.05$ if not specified.

3 Results

3.1 Prognosis-related angiogenic genes in the TCGA-BLCA cohort

To commence, we selected 268 ARGs from ten distinct angiogenesis-related gene sets as a reference for subsequent investigations. The expression levels of these genes were compared between tumor and normal tissues using the TCGA-BLCA dataset, resulting in the identification of 45 DEGs (Fig. 1A). We conducted uniCox analysis to assess the prognostic significance of the 268 ARGs in BLCA patients, ultimately identifying 29 genes with a p-value less than 0.05. To further refine our selection, we focused on the 16 ARGs that intersected between the 45 DEGs and the 29 genes associated with survival (Supplementary Table 2). The survival implications of these intersected genes in BLCA patients are depicted in Fig. 1B. Figure 1C illustrates the predominant low expression levels of these intersected genes in the tumor samples.

3.2 Formation of ARG clusters in BLCA

Using the expression profiles of the 16 intersecting genes obtained from a total of 859 BLCA patients across the TCGA-BCLA, GSE13507, GSE31684, and GSE48276 cohorts, we conducted unsupervised consensus clustering analysis to identify distinct angiogenesis subtypes. Notably, we found that K=2 represented a relatively stable demarcation, as evidenced by the decreasing clustering stability from K=2 to K=9 (Fig. 2A and Supplementary Fig. 2). Additionally, unsupervised consensus clustering analysis on individual cohort also demonstrated that at K=2, patients within each dataset could be effectively assigned to two distinct clusters (Supplementary Fig. 3). BLCA patients from the meta cohort were clearly segregated into two clusters, namely ARG_cluster_A (n=358) and ARG_cluster_B (n=501). Furthermore, the results of principal component analysis (PCA) provided additional validation by showing a significant intergroup distribution (Fig. 2B). K–M analysis revealed that patients in ARG_cluster_A exhibited significantly shorter OS compared to those in ARG_cluster_B (Fig. 2C). Moreover, the comparison of genomic expression and clinicopathological variables between the two clusters (Fig. 2D) demonstrated that ARG_cluster_A was associated with higher levels of clinicopathological characteristics, such as higher tumor grade and more advanced lymph node or visceral metastases.

3.3 Differences in TME characteristics between ARG clusters

The GSVA analysis revealed that ARG_cluster_A exhibited a higher abundance of inflammation-related pathways, including leukocyte transendothelial migration, chemokine signaling, and cytokine-cytokine receptor interaction. Additionally, metastasis-related pathways such as ECM receptor interaction, regulation of cell adhesion molecules, and focal adhesion were found to be overexpressed in ARG_cluster_A (Fig. 3A and Supplementary Table 3). To investigate the association between ARGs and the TME in BLCA, we assessed the expression levels of ICPs in the two clusters. Notably, the expression of PD-L1, PD-1, and CTLA-4 was significantly higher in cluster A compared to cluster B (Fig. 3B–D). Using the ESTIMATE algorithm, we evaluated the abundance of immune and stromal elements in the TME by calculating TME scores, which included stromal score, immune score, and estimate score. ARG_cluster_A exhibited higher scores, indicating a more enriched TME (Fig. 3E). Furthermore, we utilized the CIBERSORT algorithm to investigate the infiltration levels of 23 human immune cell subpopulations in the two clusters, revealing notable differences in the enrichment levels of most immune cells (Fig. 3F and Supplementary Table 4). The levels of activated B cells, activated CD4 T cells, activated CD8 T cells, activated DC cells, CD56 bright NK cells, GD T cells, immature B cells, immature DC cells, MDSCs, macrophages, mast cells, NK T cells, NK cells, neutrophils, plasmacytoid DC cells, regulatory T cells, T follicular helper cells, type 1 T helper cells,

Fig. 1 Identified survival related different expressed ARGs with the TCGA-BCLA dataset. **A** The expression of 45 ARGs between tumor and non-tumor tissues in the TCGA-BCLA dataset. **B** 16 intersect ARGs between 45 DEGs and 29 survival related genes. **C** The expression of 16 interested ARGs between tumor and non-tumor tissues. Statistical significance is denoted by *p < 0.05; **p < 0.01; ***p < 0.001

type 2 T helper cells, and type 17 T helper cells were significantly higher in ARG_cluster_A compared to ARG_cluster_B. Conversely, CD56 dim NK cells and monocytes exhibited an opposite pattern of enrichment.

3.4 Identification of gene subtypes based on DEGs between ARG clusters

To gain a deeper understanding of the role of angiogenesis signaling in BLCA, we identified 482 DEGs associated with the ARG clusters. Functional enrichment analysis of these DEGs highlights the enrichment of metastasis-related biological processes, including extracellular matrix (ECM) receptor interactions and focal adhesion, suggesting that ARGs play a pivotal role in tumor invasion and metastasis (Fig. 4A and Supplementary Table 5). Additionally, KEGG analysis indicated that the abundance of pathways associated with metastasis (Fig. 4B). To further explore the prognostic relevance of these genes, we conducted uniCox analysis and identified 188 genes significantly associated with survival ($p < 0.001$) (Supplementary Table 6). To uncover specific regulatory mechanisms, we employed a consensus clustering method to classify patients into two subtypes, namely Gene_subtype_A and Gene_subtype_B, based on these prognostic genes (Supplementary Fig. 4). Gene_subtype_A exhibited a correlation with higher tumor grade, advanced T-, N-, and M-stage (Fig. 4C). These findings establish a mechanistic link between angiogenesis-related signaling and aggressive clinical features, aligning with the observed associations between ARG clusters and advanced TNM stages. Furthermore, K–M curves revealed poorer OS in patients belonging to Gene_subtype_A (Fig. 4D). Moreover, notable discrepancies in the expression of ARGs were observed between Gene_subtype_A and Gene_subtype_B, consistent with the patterns observed in the ARG clusters (Fig. 4E).

3.5 Construction of the ARG score and it's prognostic value

We utilized LASSO and multivariate Cox analysis based on the 188 prognostic DEGs associated with the ARG clusters to establish an optimal predictive model (Supplementary Fig. 5). Ultimately, we identified ten genes (MFAP5, OLFML2B, CD109, EMP1, THBS2, BCT1, FBP1, COMP, TM4SF1, and CTSE) and utilized them to construct the ARG score. An alluvial diagram illustrates the relatively consistent distribution of patients in the two ARG clusters, two Gene subtypes, and two ARG score groups (Fig. 5A). Consistently, significant differences in the ARG score were observed between both ARG clusters and Gene subtypes (Fig. 5B, C). K–M analysis demonstrated that patients with lower ARG scores had better OS compared to those with higher scores (Fig. 5D). Different distributions of ARG scores among different ARG clusters were also observed in individual cohorts. Furthermore, significant survival differences between high and low ARG scores were observed in all cohorts except for the GSE31684 (Supplementary Fig. 6). The AUC for predicting 1-, 3-, and 5-year OS was 0.705, 0.701, and 0.702, respectively (Fig. 5E). Additionally, PCA unveiled a distinct separation between the two ARG score groups (Fig. 5F). The risk plot of the ARG score suggests that as the score increases, OS decreases while mortality increases (Fig. 5G, H). A heatmap displaying the expression patterns of the selected ten genes is presented in Fig. 5I.

3.6 TME and immune checkpoints in high and low ARG score groups

As depicted in Fig. 6A, ARG score exhibited a positive correlation with the infiltration of resting CD4 memory T cells, follicular helper T cells, activated NK cells, Macrophages M0, Macrophages M1, Macrophages M2, resting dendritic cells, resting mast cells, and neutrophils. Conversely, a negative correlation was observed between the ARG score and naive B cells, plasma cells, CD8+ T cells, T cells CD4+ naive, activated CD4+ memory T cells, regulatory T cells (Tregs), resting NK cells, and activated dendritic cells. We also assessed the correlation between the genes included in the ARG score scoring system and the levels of immune cell enrichment. The analysis revealed significant associations between the selected genes and the majority of immune cell populations (Fig. 6B). Next, we evaluated the abundance of immune and stromal elements in the TME of the two ARG score groups, and observed a positive correlation between the ARG score and stromal score, as well as immune score (Fig. 6C). Additionally, we examined the relationship between 28 ICPs and the ARG score (Fig. 6D), which demonstrated that most ICPs exhibited higher expression in the high ARG score group, with the exception of CD40, CD160, TNFRSF14, CEACAM1, BTN2A1, and CD96.

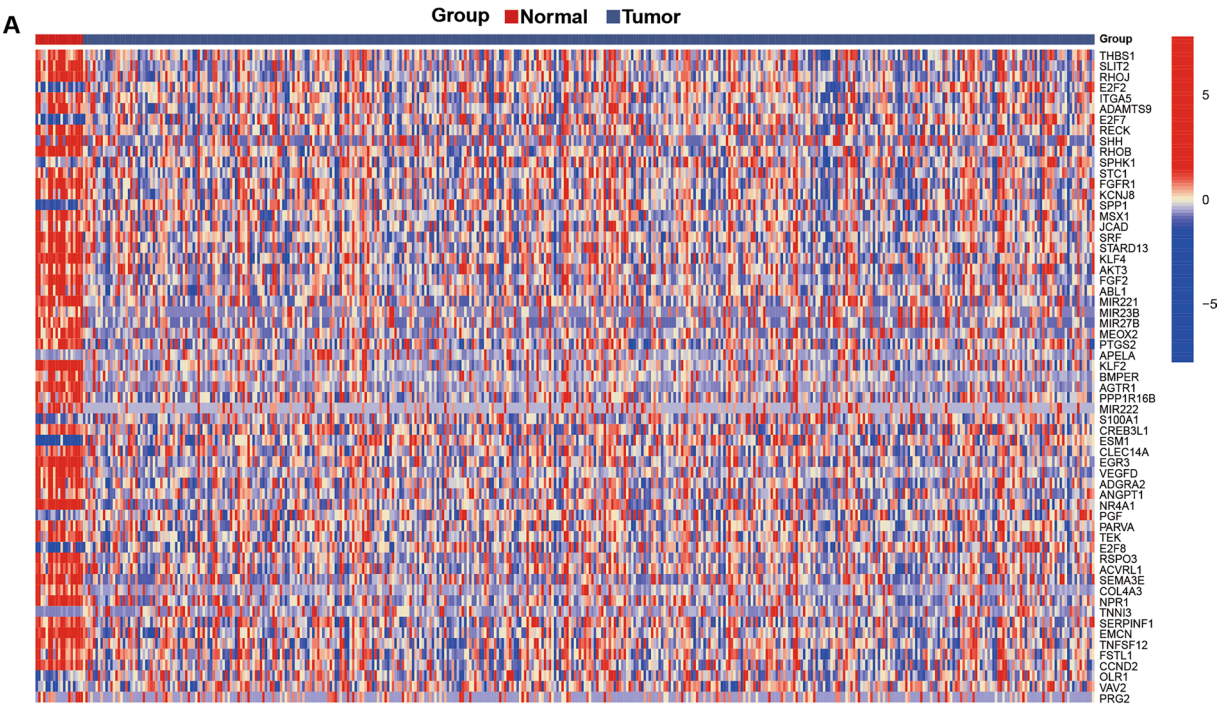
A
Group Normal Tumor
Group
THBS1
SLIT2
RHOJ
E2F2
ITGA5
ADAMTS9
E2F7
RECK
SHH
RHOB
SPHK1
STC1
FGFR1
KCNJ8
SPP1
MSX1
JCAD
SRF
STARD13
KLF4
AKT3
FGF2
ABL1
MIR221
MIR23B
MIR27B
MEOX2
PTGS2
APELA
KLF2
BMPER
AGTR1
PPP1R16B
MIR222
S100A1
CREB3L1
ESM1
CLEC14A
EGR3
VEGFD
ADGRA2
ANGPT1
NR4A1
PGF
PARVA
TEK
E2F8
RSPO3
ACVRL1
SEMA3E
COL4A3
NPR1
TNNI3
SERPINF1
EMCN
TNFSF12
FSTL1
CCND2
OLR1
VAV2
PRG2
5
0
−5

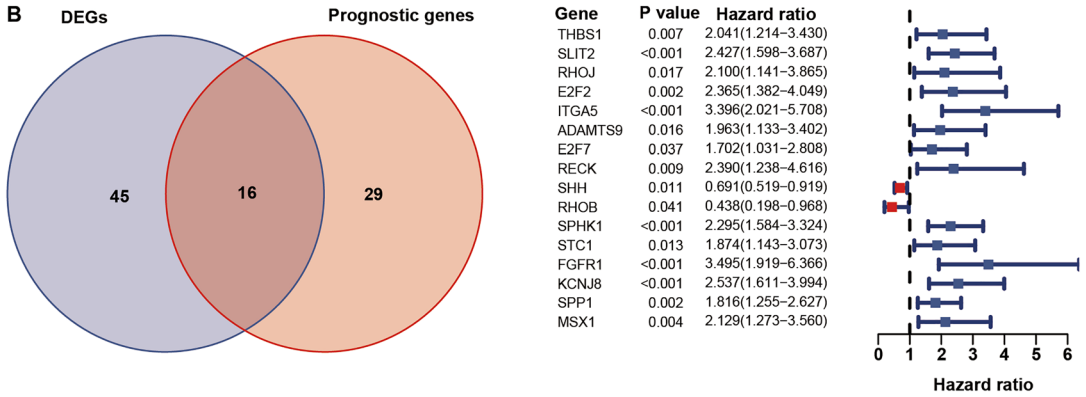
B
DEGs
Prognostic genes
45
16
29
Gene P value Hazard ratio
THBS1 0.007 2.041(1.214−3.430)
SLIT2 <0.001 2.427(1.598−3.687)
RHOJ 0.017 2.100(1.141−3.865)
E2F2 0.002 2.365(1.382−4.049)
ITGA5 <0.001 3.396(2.021−5.708)
ADAMTS9 0.016 1.963(1.133−3.402)
E2F7 0.037 1.702(1.031−2.808)
RECK 0.009 2.390(1.238−4.616)
SHH 0.011 0.691(0.519−0.919)
RHOB 0.041 0.438(0.198−0.968)
SPHK1 <0.001 2.295(1.584−3.324)
STC1 0.013 1.874(1.143−3.073)
FGFR1 <0.001 3.495(1.919−6.366)
KCNJ8 <0.001 2.537(1.611−3.994)
SPP1 0.002 1.816(1.255−2.627)
MSX1 0.004 2.129(1.273−3.560)
0 1 2 3 4 5 6
Hazard ratio

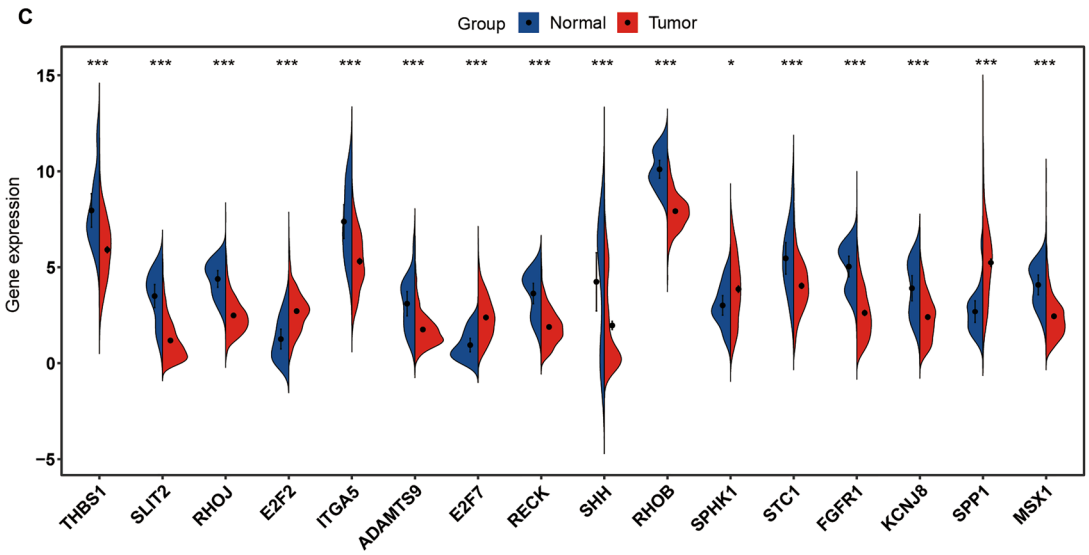
C
Group Normal Tumor
Gene expression
15
10
5
0
−5
THBS1 SLIT2 RHOJ E2F2 ITGA5 ADAMTS9 E2F7 RECK SHH RHOB SPHK1 STC1 FGFR1 KCNJ8 SPP1 MSX1

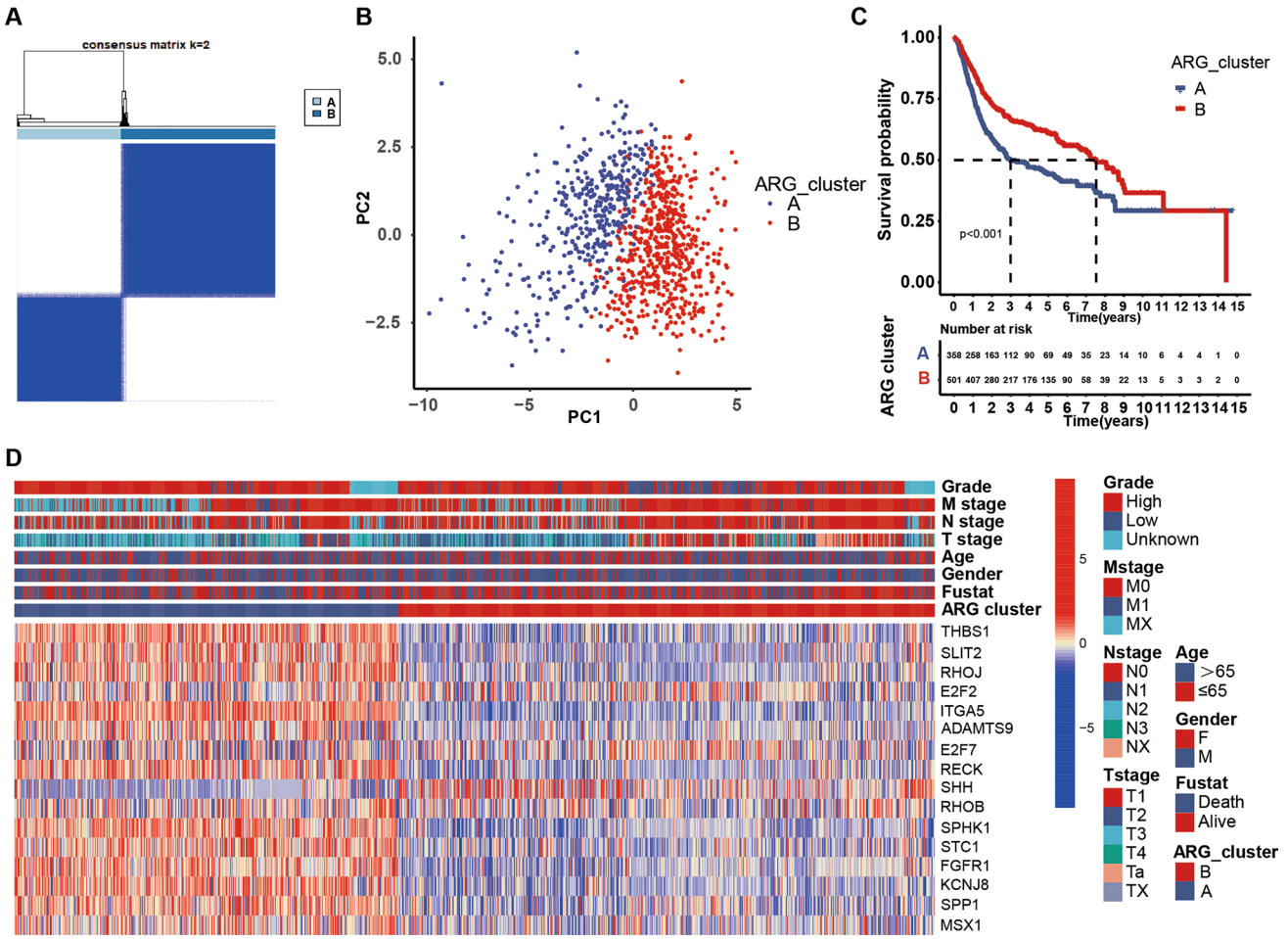

Fig. 2 ARG clusters and the corresponding overall survival and clinical pathological features. **A** Consensus matrix heatmap defining two clusters (k = 2) and their correlation area. **B** PCA analysis revealed distinct transcriptomic differences between the two clusters. **C** K–M curves demonstrated significant differences in OS between the ARG clusters. **D** The expression levels of the 16 ARGs across the two ARG clusters and their associations with age, gender, fustat (alive or deceased at the last follow-up), clinical TNM stage (tumor size/invasion, lymph node involvement, and metastasis), and pathological grade (low-grade versus high-grade tumors)

3.7 Association between ARG score and TMB

To investigate the potential correlation between the ARG score and TMB, we performed a Spearman correlation analysis. The results indicated no significant linear relationship between the two variables (Fig. 7A). Similarly, a comparison of TMB between the low ARG score group and the high ARG score group revealed no significant difference (Fig. 7B). In addition, we examined the distribution of somatic mutations between the two ARG score groups using the TCGA-BLCA dataset. The mutation incidences of TP53, TTN, KMT2D, MUC16, and ARID1A were found to be equal to or higher than 20% across both ARG score groups (Fig. 7C–D). Notably, TP53, RB1, KMT2D, RB1, and EP300 were more frequently mutated in the high ARG score group. These genes are known to be involved in tumor progression and may influence angiogenesis by modulating extracellular matrix remodeling and angiogenic signaling. Conversely, mutations such as those in KDM6A, which were more frequent in the low ARG score group, are associated with epigenetic regulation and could suppress angiogenesis-related activity. These findings suggest a potential mechanistic link between these mutations and the regulation of the ARG score, warranting further investigation.

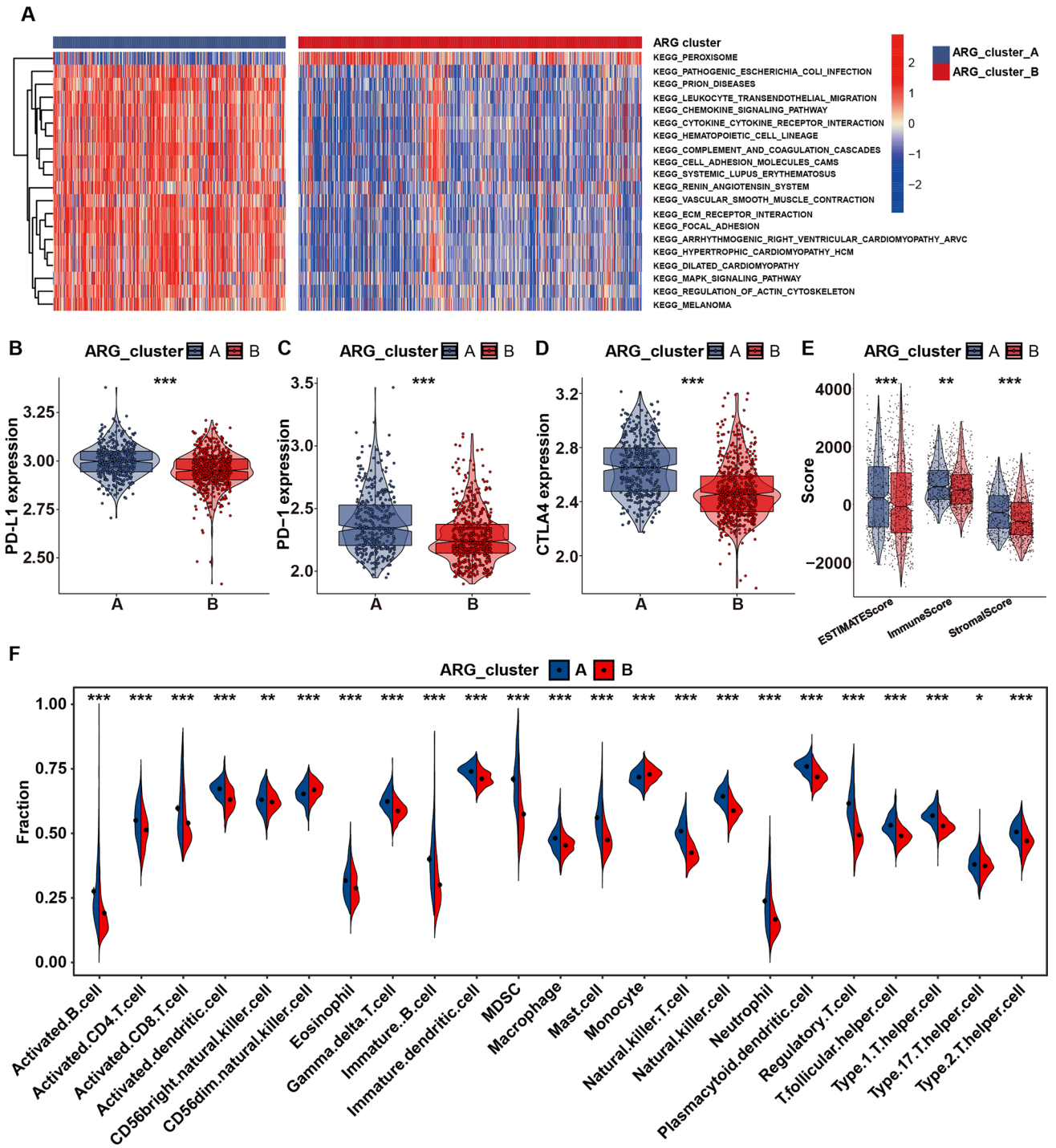

Fig. 3 Intersection between TMB and ARG clusters. **A** Gene set variation analysis is employed to compare the activity of biological pathways between the ARG clusters. **B**–**D** The expression of immune checkpoint molecules between the ARG clusters were compared. **E** The distribution of TME scores among different ARG clusters. **F** The abundance of 23 infiltrating immune cell types between the ARG clusters. Statistical significance is denoted by *p < 0.05; **p < 0.01; ***p < 0.001

3.8 Drug sensitivity analysis

For muscle-invasive BLCA, chemotherapy and immunotherapy are two primary systemic treatment modalities. We calculated the immune prognostic score (IPS) to predict their ability to respond to these treatments. As depicted in

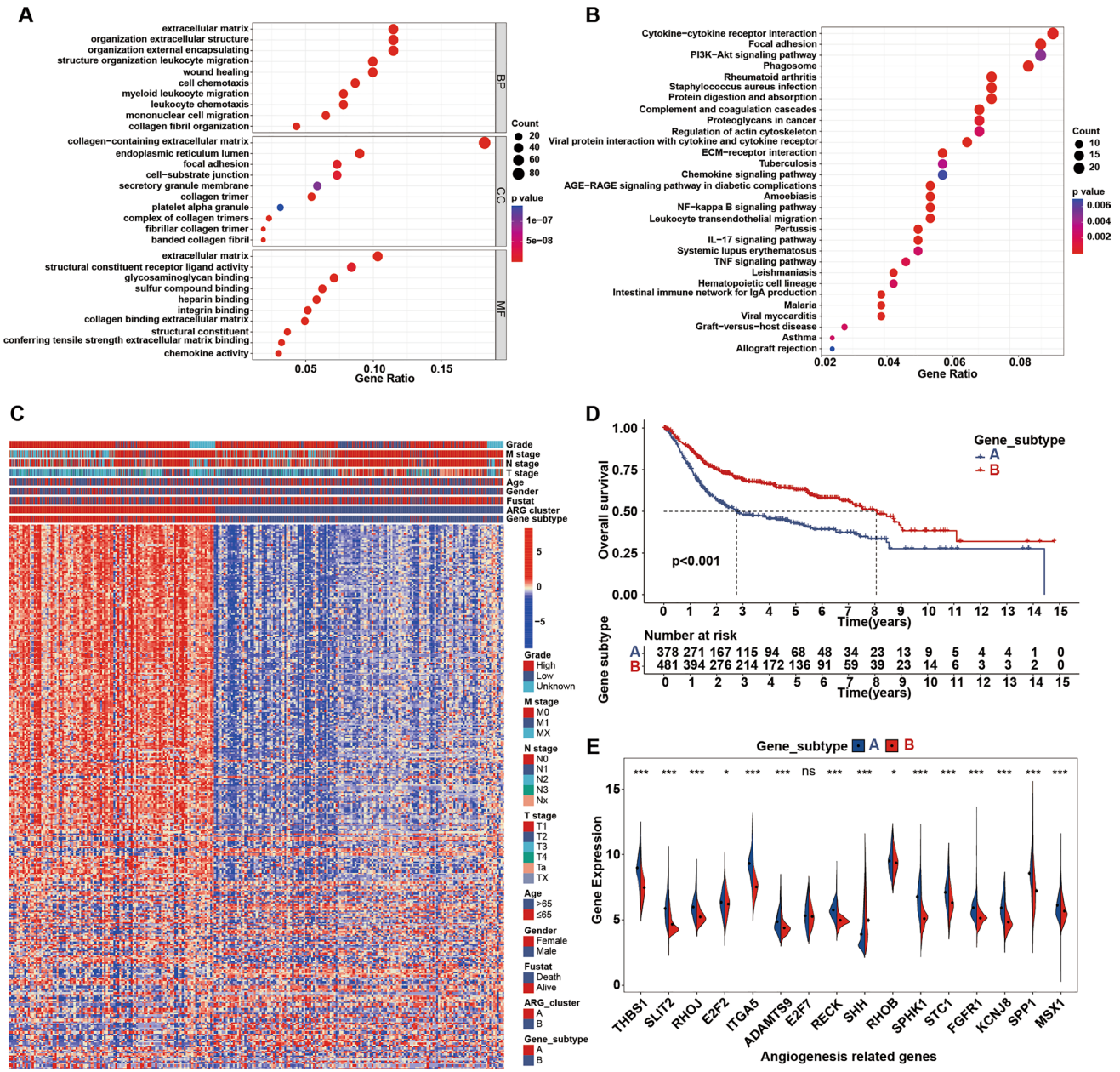

Fig. 4 Identifying gene subtypes based on DEGs associated with the ARG clusters. **A**, **B** GO and KEGG enrichment analyses of DEGs between the two ARG cluster reveal significant involvement of metastasis-related pathways, such as ECM receptor interaction and regulation of cell adhesion molecules. **C** Differential gene expression and clinical pathological features between the two Gene subtypes. **D** K–M curves for OS of the two Gene subtypes. **E** The expression of 16 ARGs among the two Gene subtypes. Statistical significance is denoted by *p < 0.05; **p < 0.01; ***p < 0.001

Fig. 8A–D, high ARG score groups exhibited higher IPS scores, suggesting that patients with a high ARG score may display increased sensitivity to immunotherapy. Subsequently, we evaluated the effectiveness of the ARG score as a biomarker for predicting therapeutic response in BLCA patients by estimating the IC50 values of six commonly used chemotherapy agents. The results revealed that patients with a low ARG score might exhibit more positive responses to cisplatin, vinblastine, and doxorubicin (Fig. 8E–J). To further investigate the predictive ability of ARG scores for immunotherapy efficacy, we divided post-immunotherapy patients into responsive groups, including complete response and partial response, and non-responsive groups, including stable disease and progressive disease. We found that in the IMvigor210, GSE100797, and GSE173839 cohorts, the high ARG score group had significantly more responsive patients ($p < 0.05$). While not reaching statistical significance, in the GSE111636 cohorts, patients

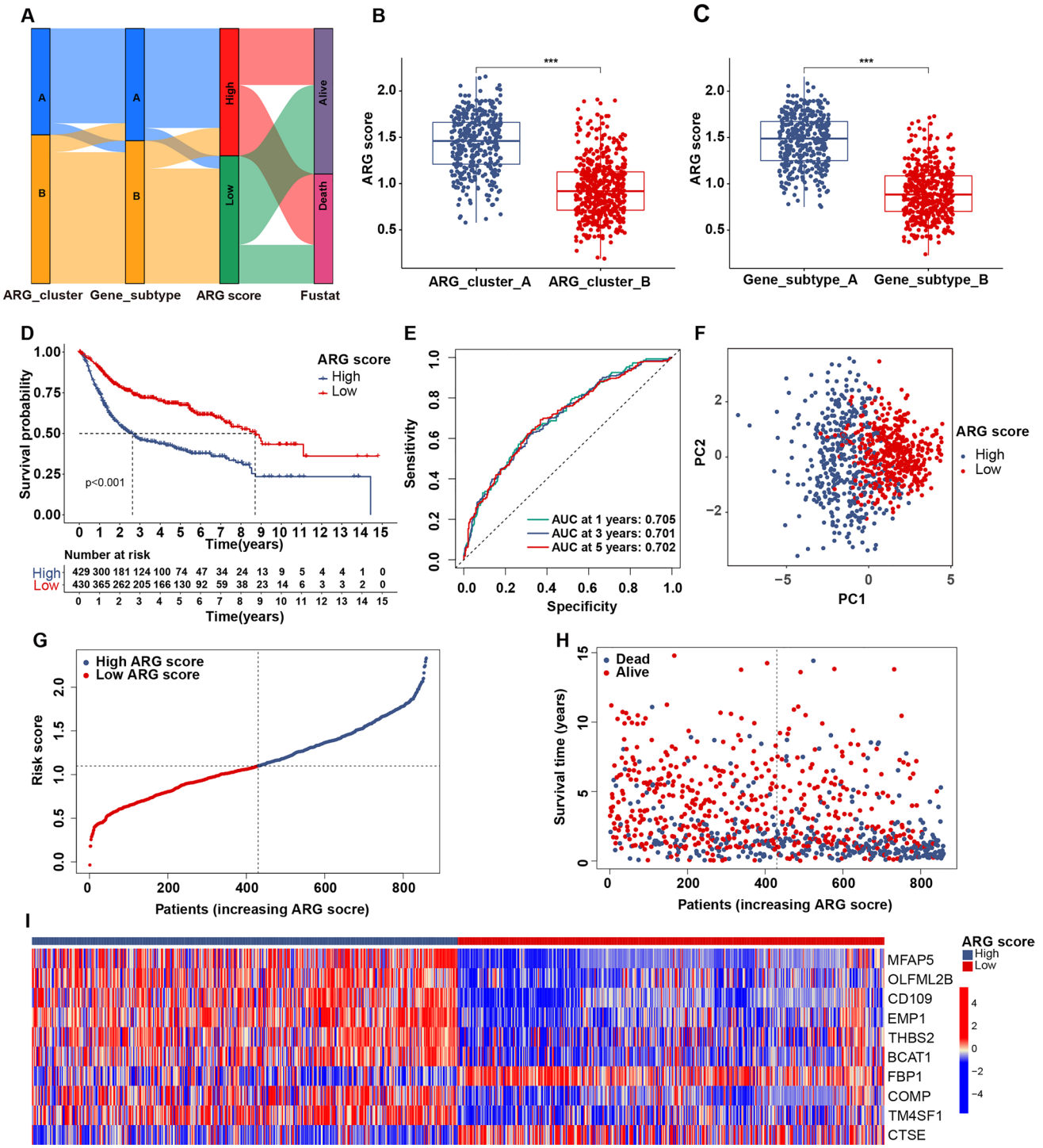

Fig. 5 The construction and evaluation of the ARG score. **A** An alluvial diagram based on the distribution of patients in the two ARG clusters, two Gene subtypes, and two ARG score groups. **B**–**C** The boxplot displays the differences in ARG scores between the ARG clusters and the Gene subtypes. **D** K–M analysis depicts the overall survival of the two ARG score groups. **E** ROC curves show the predictive performance of the ARG score for 1-, 3-, and 5-year overall survival. **F** Principal component analysis visualizes the distinct differences between the two ARG score groups. **G**, **H** Ranked dot plot and scatter plot displayed the relationship between ARG score and the risk of mortality, as well as the association between ARG score and survival time. **I** The heatmap depicts the expression of ten selected prognostic genes in the high and low ARG score groups

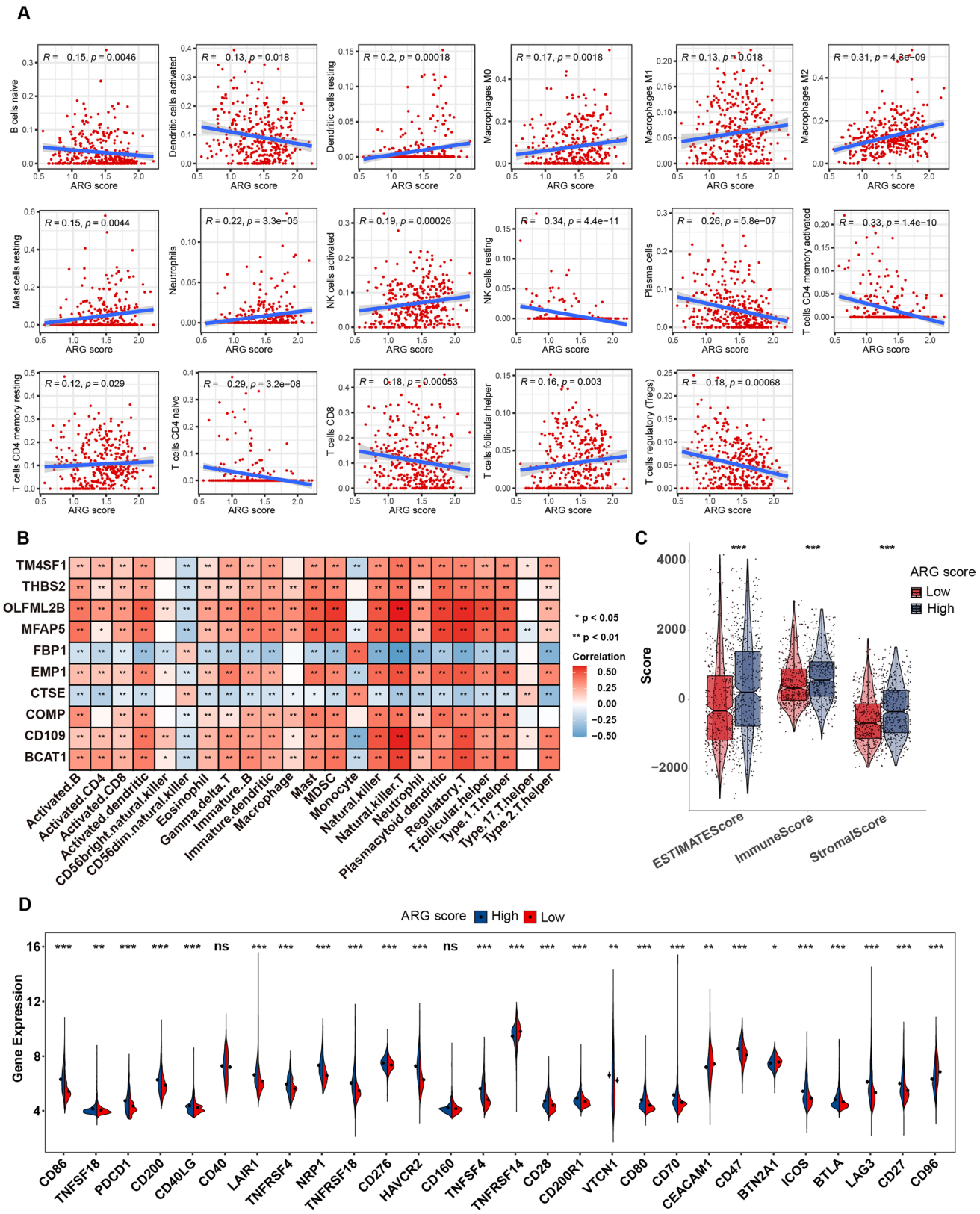

Fig. 6 The heterogeneity of the TME and immune checkpoints between the high and low ARG score groups. **A** Correlations between immune cell and ARG score. **B** The correlation between immune cell abundance and selected genes in the ARG score scoring system. **C** The correlation between ARG score and immune score as well as stromal score. **D** Expression of immune checkpoints genes in the high and low ARG score groups. Statistical significance is denoted by *p < 0.05; **p < 0.01; ***p < 0.001

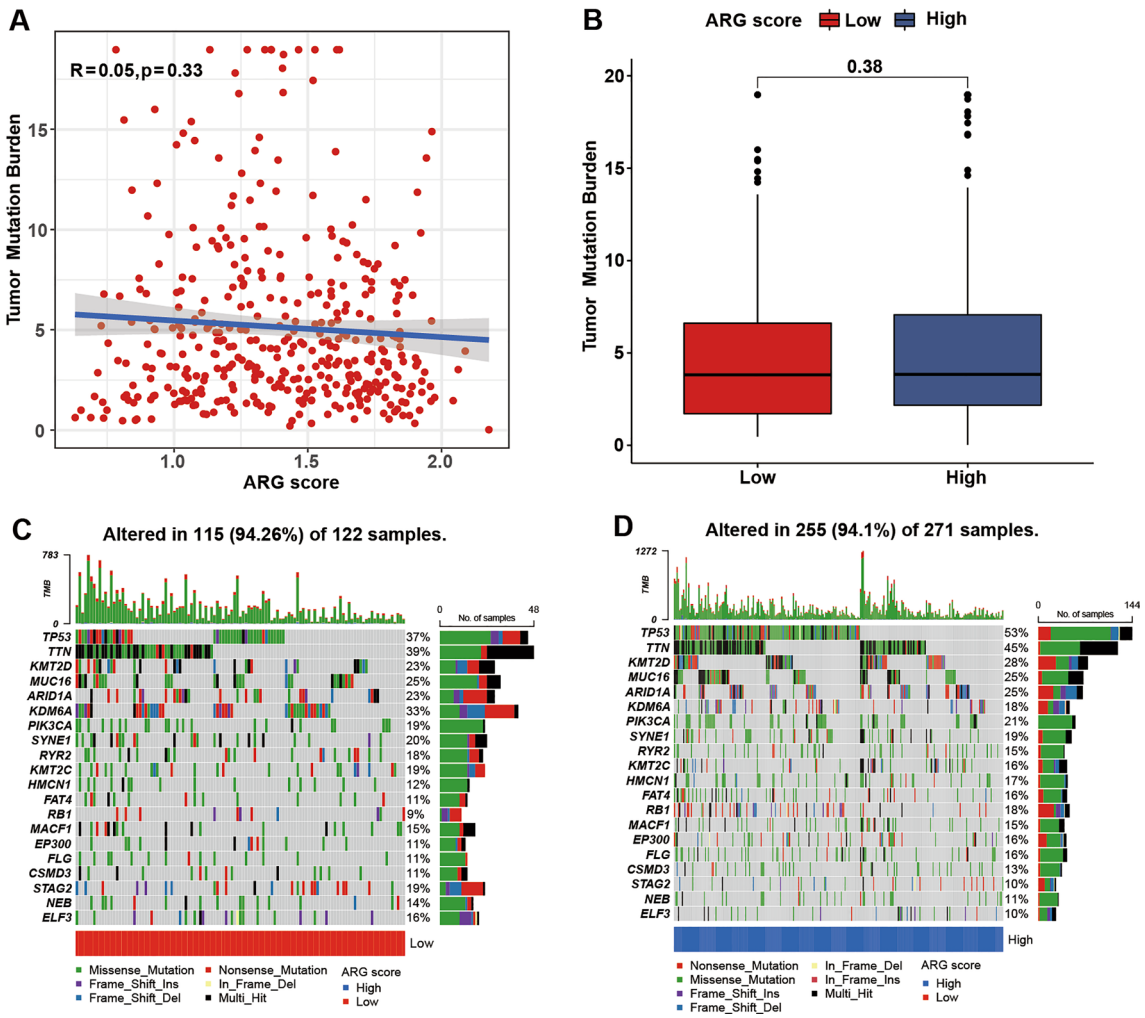

Fig. 7 **A**, **B** Relationships between ARG score and tumor mutational burden. **C**, **D** The waterfall plot of somatic mutation features established with high and low ARG score

in the high ARG score group exhibited an increasing trend in response rates to immunotherapy. (Fig. 8K–N). These findings collectively indicate a correlation between ARG score and drug sensitivity, providing valuable insights into personalized treatment approaches for BLCA.

3.9 Construction of patient prognosis nomogram

Given the strong correlation between ARG score and patient prognosis, we constructed a nomogram incorporating clinical parameters to assess the 3-year, 5-year, and 10-year OS of BLCA patients (Fig. 9A). The calibration curves of the nomogram demonstrated high accuracy, indicating a close agreement between the predicted and observed outcomes (Fig. 9B–D). Comparisons between the prognostic model incorporating the ARG score and the model based solely on clinicopathologic characteristics revealed that the former provided greater net benefits in survival prediction (Fig. 9E–G). The AUC was further compared to assess the predictive performance of the two models in overall patients and patients with different T stages. As shown in Fig. 9H–J and Supplement Fig. 7, the model incorporating the ARG score demonstrated a more accurate predictive ability for the prognosis of BLCA.

3.10 Preliminary functional verification of CD109 and TM4SF1

In the ARG score rating system, the genes found to be overexpressed, CD109 and TM4SF1, had the highest weighting coefficients. Therefore, initial validation of the functions of these two genes was conducted. qRT-PCR results showed a

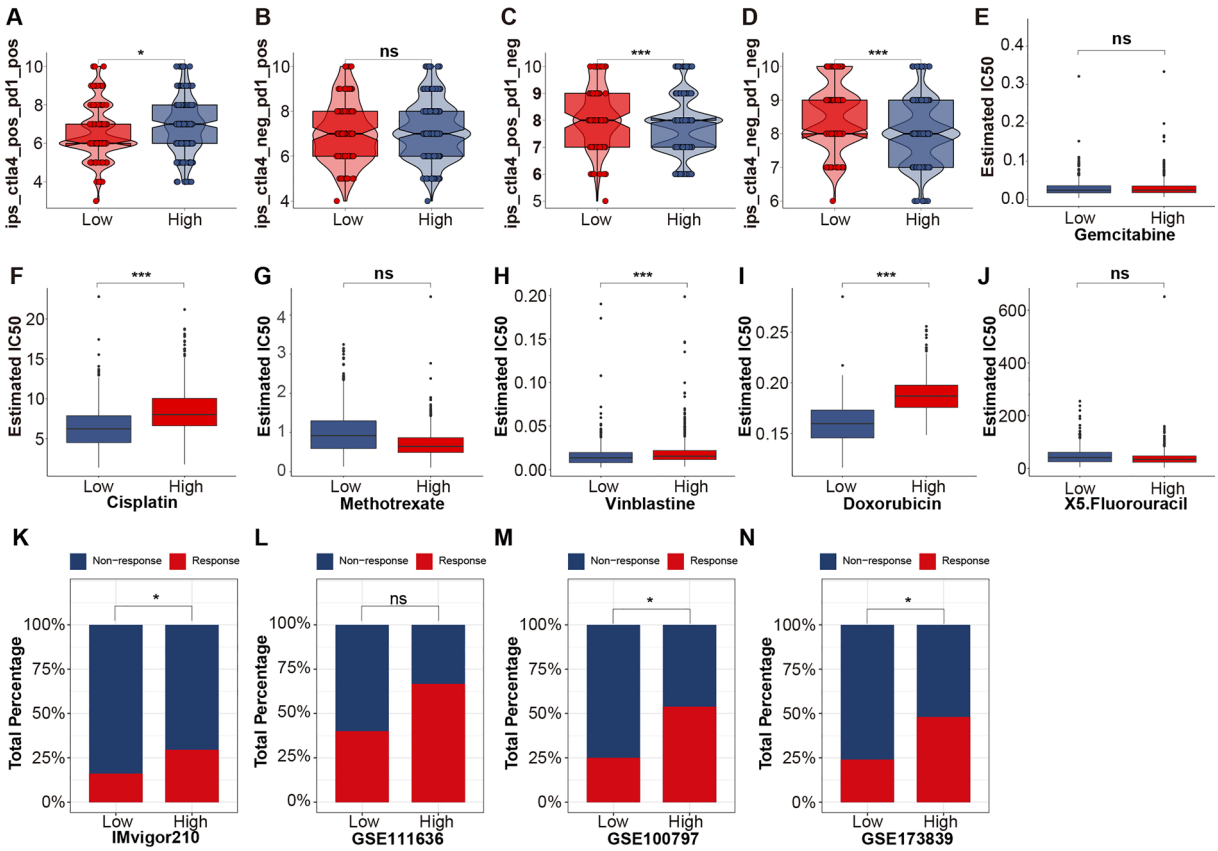

Fig. 8 Relationships between ARG score and therapeutic sensitivity. **A**–**D** IPS in different ARG score groups. **F**–**J** Relationships between ARG score and chemotherapeutic sensitivity. **K**–**N** ARG score for predicting immunotherapy efficacy in different cohorts. Statistical significance is denoted by *p < 0.05; **p < 0.01; ***p < 0.001; *ns* no significant. Low and high represent low ARG score and high ARG score, respectively

significant reduction in the expression levels of CD109 and TM4SF1 after siRNA transfection (Fig. 10A, B). As expected, CCK-8 assays confirmed that silencing CD109 or TM4SF1 significantly inhibited the proliferation capability of 5637 cells (Fig. 10C). Furthermore, interference with CD109 or TM4SF1 expression suppressed colony formation (Fig. 10D, E). Additionally, 5637 cell migration, as well as invasiveness, also showed a decreased tendency after knockdown of CD109 or TM4SF1 compared to those transfected with si-NC, as measured by wound healing and transwell assays (Fig. 10F–I).

4 Discussion

Angiogenic cytokines serve as drivers of angiogenesis and immunomodulators, playing a crucial role in the progression of BLCA [20]. These cytokines can activate the angiogenic switch that promotes tumor progression, establish autocrine pathways that regulate tumor progression through the activation of endothelial cells [21]. Furthermore, angiogenic cytokines can also inhibit antigen-presenting cells and immune effector cells, activate immune-suppressive cells, and exert immunosuppressive effects. This inhibitory effect can further stimulate angiogenesis, creating a vicious cycle [22]. The inherent connection between angiogenesis and immune regulation suggests that angiogenic features may serve as crucial predictive factors for the efficacy of tumor immunotherapy [23, 24].

In this study, by clustering BLCA patients into two ARG clusters using unsupervised clustering, we identified significant differences in clinical outcomes, immune infiltration patterns, and functional characteristics between the clusters. By analyzing DEGs between the ARG clusters and performing enrichment analysis on these DEGs, we observed the enrichment of metastasis-related pathways, such as ECM receptor interaction and focal adhesion, indicating the role of ARGs in promoting tumor invasion and progression. Subsequently, using the DEGs between the two ARG clusters, we identified two gene subgroups in BLCA and validated their differences in clinical-pathological characteristics, immune activity, and functions. To quantify the angiogenesis-related features of each cluster, an ARG score was established

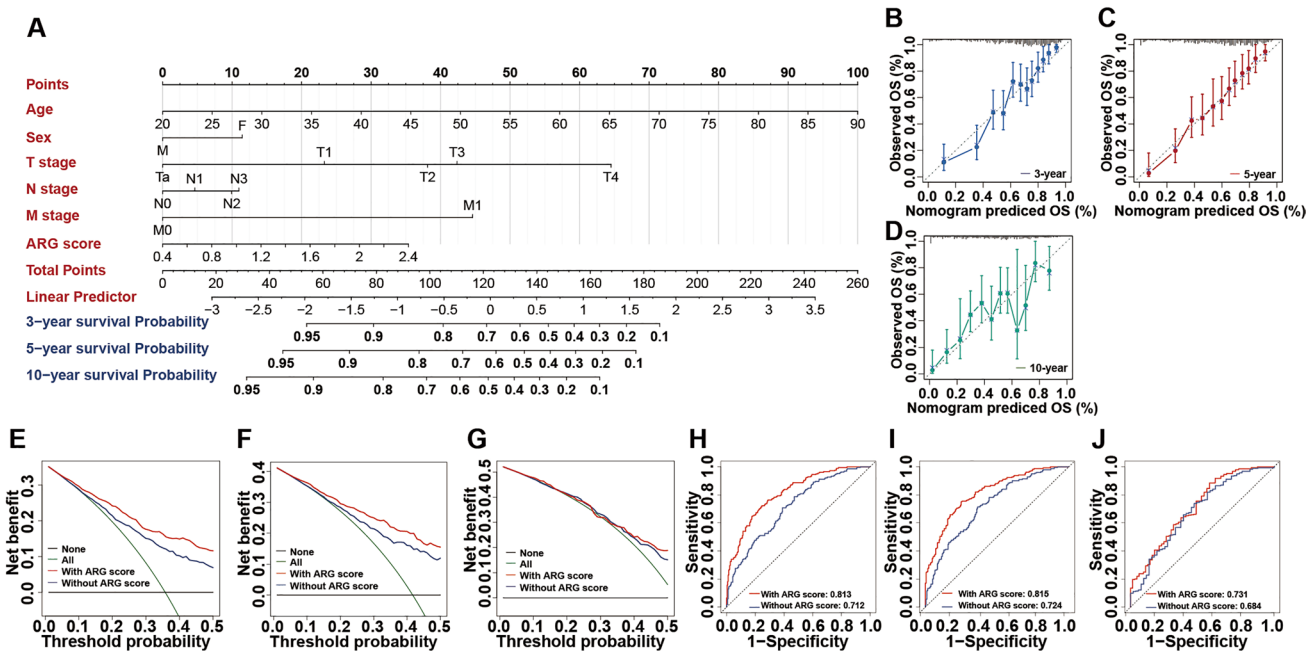

Fig. 9 Nomogram and its predictive performance evaluation. **A** Nomogram for predicting the 3-, 5-, and 10-year overall survival of bladder cancer patients. **B**–**D** Evaluation of predictive accuracy of nomogram for the 3-, 5-, and 10-year survival by correction curves. **E**–**G** Comparing the accuracy of different models in predicting 3, 5, and 10-year overall survival through the decision curve analysis curves. **H**–**J** Comparing the accuracy of different models in predicting 3, 5, and 10-year overall survival through time dependent receiver operating characteristic curves

using LASSO-Cox regression. A high ARG score was significantly associated with poor OS, indicating its potential as a prognostic predictor. Angiogenesis has been identified as a critical factor in the progression of various cancers, including BLCA [25, 26]. A systematic review and meta-analysis of 17 studies investigated the impact of microvessel density on the prognosis of BLCA. The results showed a significant association between high microvessel density and poor OS and disease-free survival [27]. Then, GSEA results demonstrate significant enrichment of inflammation and metastasis-related pathways in the group with high ARG expression. Additionally, the higher ARG score showed a significant correlation with advanced clinical-pathological characteristics of BLCA. ROC analysis validated the accuracy of the ARG score in predicting OS. After adjusting for confounding variables through multivariate COX regression, the ARG score remained an independent predictor of OS in BLCA patients. These findings suggest that the ARG score holds promise as a reliable tool for assessing patient prognosis.

Accumulation of gene mutations plays a crucial role in tumor development. In our study, we did not observe significant differences in the total mutation burden between patients with high ARG scores and those with low ARG scores. However, the observed mutations in TP53, TTN, and KMT2D in the high ARG score group provide important insights into the genetic underpinnings of enhanced angiogenesis in BLCA. TP53 mutations, frequently associated with loss of tumor suppressor function, may lead to increased angiogenic activity through the upregulation of VEGF signaling and hypoxia-induced pathways [28]. Similarly, RB1 mutations, known for their role in cell cycle regulation, may contribute to tumor progression and indirectly promote angiogenesis by fostering an aggressive tumor microenvironment [29]. KMT2D mutations, which affect chromatin remodeling, can activate oncogenic transcriptional programs, including those linked to angiogenic pathways and immune tolerance [30]. In contrast, KDM6A mutations, more prevalent in the low ARG score group, are linked to epigenetic modifications that may suppress angiogenic gene expression [31]. These findings suggest that genetic alterations could play a pivotal role in shaping the angiogenesis landscape, as reflected by the ARG score. Further functional studies are required to validate these associations and explore their potential as therapeutic targets. Due to the higher tumor mutation burden in BLCA, ICIs have shown good efficacy in some patients. Currently, the US Food and Drug Administration has approved five ICIs for BLCA management [32]. Rosenberg et al. first reported the results of atezolizumab in the treatment of advanced BLCA, with an overall objective response rate (ORR) of 15%. The study also indicated a correlation between TCGA molecular subtypes and the effectiveness of immunotherapy [33]. Furthermore, Nivolumab achieved an overall ORR of 19.6% in metastatic urothelial carcinoma after platinum-based

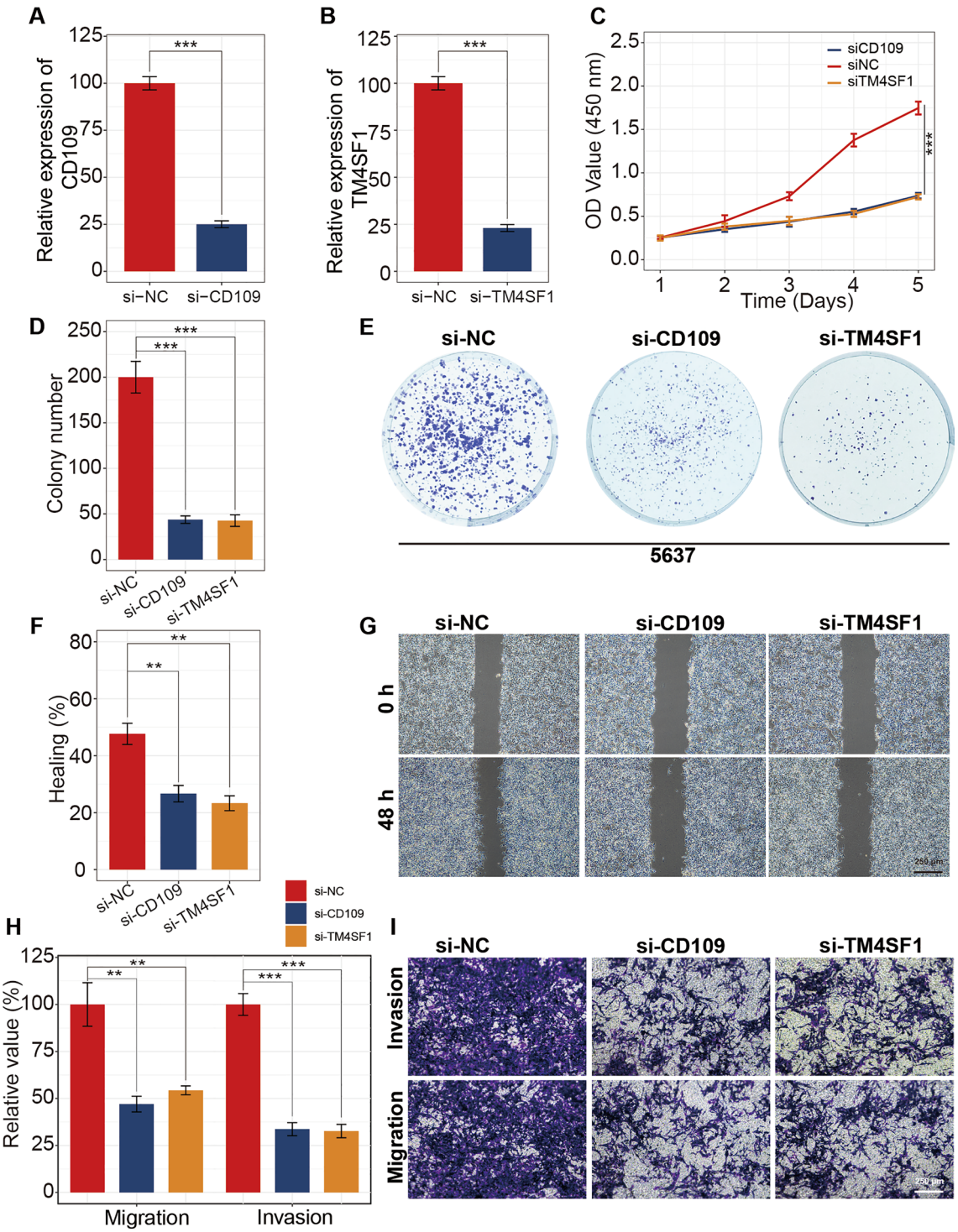

Fig. 10 CD109, TM4SF1 promote the proliferation and migration of bladder cancer cells. **A**, **B** The relative expression of CD109 and TM4SF1 in 5637 cells after transferring with si-CD109 and si-TM4SF1 was determined by qRT-PCR. **C**–**E** The proliferation of 5637 cells transfected with siRNA against CD109 or TM4SF1 were measured using CCK-8 and colony formation assays. **F**, **G** Effects of CD109 and TM4SF1 downregulation on bladder cancer cell migration, as evaluated by wound healing assay. **H**, **I** Transwell assays were applied to determine the migration and invasion capacity of 5637 cells after CD109 or TM4SF1 downregulation. Statistical significance is denoted by *$p < 0.05$; **$p < 0.01$; ***$p < 0.001$

chemotherapy [34]; Pembrolizumab as a second-line treatment for advanced BLCA significantly improved OS [35]. These clinical studies highlight the critical role of ICIs while also indicating that not all patients respond to ICI treatment. Tumor responsiveness to immunotherapy is closely related to its internal TME, consisting of stromal cells and immune cells, and its impact on BLCA treatment outcomes has been confirmed in previous studies [36–38]. In this study, we used the ESTIMATE algorithm to calculate TME-related scores and found that the high ARG score group exhibited higher immune and stromal scores compared to the low ARG score group. This suggests that angiogenesis may influence the development of BLCA by interacting with the TME. Additionally, we observed that in patients with low ARG scores, there was a higher enrichment of T cells (helper T cells, CD4+, and CD8+ T cells) and dendritic cells, while the number of Tregs found in the TME increased with higher ARG scores, which was associated with poorer survival rates [39]. These results further support the previously reported interaction between angiogenic factors and the immune microenvironment [40, 41]. Therefore, targeting angiogenesis alongside immunotherapy may be a potential strategy to enhance the effectiveness of BLCA immunotherapy [42, 43]. In this study, we explored the relationship between the ARG score and patient sensitivity to ICI treatment. The results suggest that BLCA patients with high ARG scores exhibit better responsiveness to anti-PD1 and anti-CTLA-4 treatments. Furthermore, a positive correlation trend between high ARG scores and immunotherapy responsiveness was also observed in breast cancer, melanoma, and lung cancer cohorts. Neoadjuvant or adjuvant cisplatin-based chemotherapy is considered key in treating muscle-invasive BLCA [44]. By calculating patient IC50 values for chemotherapy drugs, we found that the low ARG score group was more sensitive to cisplatin than the high ARG score group. These results suggest that adding angiogenesis inhibitors on top of chemotherapy may yield better treatment outcomes for patients with high ARG scores.

Several limitations should be acknowledged in this study. Firstly, the retrospective nature of the data obtained from public databases introduces inherent selection bias, which may impact the robustness of the findings. Secondly, the inclusion of additional clinical variables would enhance the exploration of the clinical relevance of ARG score. Finally, further in vivo and in vitro experiments, as well as prospective clinical studies, are necessary to gain a deeper understanding of the relationship between ARG score and TME, in order to validate our findings and hypotheses.

5 Conclusions

In conclusion, our analysis of ARGs uncovers their regulatory role within the TME and their influence on the prognosis and clinical characteristics of BLCA patients. Moreover, we identify ARGs as a promising biomarker for predicting therapeutic response. These findings underscore the clinical relevance of ARGs and lay a solid groundwork for future investigations in the realm of personalized therapy for BLCA patients.

Author contributions Conceptualization—G.X and H.G; methodology—C.R; software, formal analysis, data curation, and original draft preparation—G.X; vitro experiments—J.Y. All authors have read and agreed to the published version of the manuscript.

Funding This study was supported by funding from projects of Beijing Municipal Education Commission, (XG, Grant No.M202410025014), Natural Science Foundation of Capital Medical University (XG, Grant No.YZ23072), Friendship Hospital Seed Program (XG, NO.YZZ202232).

Data availability The datasets used and/or analysed during the current study are available from the corresponding author on reasonable request.

Declarations

Institutional review board statement Not applicable.

Informed consent Not applicable.

Competing interests The authors declare no competing interests.

References

1. Lobo N, et al. Epidemiology, screening, and prevention of bladder cancer. Eur Urol Oncol. 2022;5(6):628–39.
2. Galsky MD, et al. Atezolizumab with or without chemotherapy in metastatic urothelial cancer (IMvigor130): a multicentre, randomised, placebo-controlled phase 3 trial. Lancet. 2020;395(10236):1547–57.
3. Galsky MD, et al. Randomized double-blind phase II study of maintenance pembrolizumab versus placebo after first-line chemotherapy in patients with metastatic urothelial cancer. J Clin Oncol. 2020;38(16):1797–806.
4. Wu Z, et al. Current status and future perspectives of immunotherapy in bladder cancer treatment. Sci China Life Sci. 2021;64(4):512–33.
5. Balar AV, et al. First-line pembrolizumab in cisplatin-ineligible patients with locally advanced and unresectable or metastatic urothelial cancer (KEYNOTE-052): a multicentre, single-arm, phase 2 study. Lancet Oncol. 2017;18(11):1483–92.
6. Viallard C, Larrivée B. Tumor angiogenesis and vascular normalization: alternative therapeutic targets. Angiogenesis. 2017;20(4):409–26.
7. Lugano R, Ramachandran M, Dimberg A. Tumor angiogenesis: causes, consequences, challenges and opportunities. Cell Mol Life Sci. 2020;77(9):1745–70.
8. Song Y, et al. Anti-angiogenic agents in combination with immune checkpoint inhibitors: a promising strategy for cancer treatment. Front Immunol. 2020;11:1956.
9. Yu WD, et al. Mechanisms and therapeutic potentials of cancer immunotherapy in combination with radiotherapy and/or chemotherapy. Cancer Lett. 2019;452:66–70.
10. Johnson WE, Li C, Rabinovic A. Adjusting batch effects in microarray expression data using empirical Bayes methods. Biostatistics. 2007;8(1):118–27.
11. Sabah A, et al. Enhancing web search result clustering model based on multiview multirepresentation consensus cluster ensemble (mmcc) approach. PLoS ONE. 2021;16(1): e0245264.
12. Wilkerson MD, Hayes DN. ConsensusClusterPlus: a class discovery tool with confidence assessments and item tracking. Bioinformatics. 2010;26(12):1572–3.
13. Hänzelmann S, Castelo R, Guinney J. GSVA: gene set variation analysis for microarray and RNA-seq data. BMC Bioinform. 2013;14:7.
14. Yoshihara K, et al. Inferring tumour purity and stromal and immune cell admixture from expression data. Nat Commun. 2013;4:2612.
15. Chen B, et al. Profiling tumor infiltrating immune cells with CIBERSORT. Methods Mol Biol. 2018;1711:243–59.
16. Mayakonda A, et al. Maftools: efficient and comprehensive analysis of somatic variants in cancer. Genome Res. 2018;28(11):1747–56.
17. Chalmers ZR, et al. Analysis of 100,000 human cancer genomes reveals the landscape of tumor mutational burden. Genome Med. 2017;9(1):34.
18. Geeleher P, Cox N, Huang RS. pRRophetic: an R package for prediction of clinical chemotherapeutic response from tumor gene expression levels. PLoS ONE. 2014;9(9): e107468.
19. Iasonos A, et al. How to build and interpret a nomogram for cancer prognosis. J Clin Oncol. 2008;26(8):1364–70.
20. Wigner P, et al. The interplay between oxidative stress, inflammation and angiogenesis in bladder cancer development. Int J Mol Sci. 2021. https://doi.org/10.3390/ijms22094483.
21. Sonpavde G, Bellmunt J. Bladder cancer: angiogenesis as a therapeutic target in urothelial carcinoma. Nat Rev Urol. 2016;13(6):306–7.
22. Rahma OE, Hodi FS. The intersection between tumor angiogenesis and immune suppression. Clin Cancer Res. 2019;25(18):5449–57.
23. Rivera LB, Bergers G. Intertwined regulation of angiogenesis and immunity by myeloid cells. Trends Immunol. 2015;36(4):240–9.
24. Trenti A, et al. Estrogen, angiogenesis, immunity and cell metabolism: solving the puzzle. Int J Mol Sci. 2018. https://doi.org/10.3390/ijms19030859.
25. Bochner BH, et al. Angiogenesis in bladder cancer: relationship between microvessel density and tumor prognosis. J Natl Cancer Inst. 1995;87(21):1603–12.
26. Black PC, Dinney CP. Bladder cancer angiogenesis and metastasis—translation from murine model to clinical trial. Cancer Metastasis Rev. 2007;26(3–4):623–34.
27. Huang J, et al. Microvessel density as a prognostic factor in bladder cancer: a systematic review of literature and meta-analysis. Cancer Biomark. 2014;14(6):505–14.
28. Wheler JJ, et al. TP53 alterations correlate with response to VEGF/VEGFR inhibitors: implications for targeted therapeutics. Mol Cancer Ther. 2016;15(10):2475–85.
29. Mandigo AC, et al. RB/E2F1 as a master regulator of cancer cell metabolism in advanced disease. Cancer Discov. 2021;11(9):2334–53.
30. Liu QX, et al. KMT2D mutations promoted tumor progression in diffuse large B-cell lymphoma through altering tumor-induced regulatory T cell trafficking via FBXW7-NOTCH-MYC/TGF-β1 axis. Int J Biol Sci. 2024;20(10):3972–85.
31. Qiu H, et al. KDM6A loss triggers an epigenetic switch that disrupts urothelial differentiation and drives cell proliferation in bladder cancer. Cancer Res. 2023;83(6):814–29.
32. Patel VG, Oh WK, Galsky MD. Treatment of muscle-invasive and advanced bladder cancer in 2020. CA Cancer J Clin. 2020;70(5):404–23.
33. Rosenberg JE, et al. Atezolizumab in patients with locally advanced and metastatic urothelial carcinoma who have progressed following treatment with platinum-based chemotherapy: a single-arm, multicentre, phase 2 trial. Lancet. 2016;387(10031):1909–20.
34. Sharma P, et al. Nivolumab in metastatic urothelial carcinoma after platinum therapy (CheckMate 275): a multicentre, single-arm, phase 2 trial. Lancet Oncol. 2017;18(3):312–22.
35. Bellmunt J, et al. Pembrolizumab as second-line therapy for advanced urothelial carcinoma. N Engl J Med. 2017;376(11):1015–26.
36. Wang Y, et al. Immune-related signature predicts the prognosis and immunotherapy benefit in bladder cancer. Cancer Med. 2020;9(20):7729–41.
37. Schneider AK, Chevalier MF, Derré L. The multifaceted immune regulation of bladder cancer. Nat Rev Urol. 2019;16(10):613–30.

38. Li P, et al. Identification of prognostic biomarkers associated with stromal cell infiltration in muscle-invasive bladder cancer by bioinformatics analyses. Cancer Med. 2020;9(19):7253–67.
39. Göschl L, Scheinecker C, Bonelli M. Treg cells in autoimmunity: from identification to Treg-based therapies. Semin Immunopathol. 2019;41(3):301–14.
40. Ribatti D, Crivellato E. Immune cells and angiogenesis. J Cell Mol Med. 2009;13(9a):2822–33.
41. Minton K. Connecting angiogenesis and autoimmunity. Nat Rev Immunol. 2019;19(10):596–7.
42. Hack SP, Zhu AX, Wang Y. Augmenting anticancer immunity through combined targeting of angiogenic and PD-1/PD-L1 pathways: challenges and opportunities. Front Immunol. 2020;11: 598877.
43. Lee WS, et al. Combination of anti-angiogenic therapy and immune checkpoint blockade normalizes vascular-immune crosstalk to potentiate cancer immunity. Exp Mol Med. 2020;52(9):1475–85.
44. Witjes JA, et al. European association of urology guidelines on muscle-invasive and metastatic bladder cancer: summary of the 2020 guidelines. Eur Urol. 2021;79(1):82–104.